Type III interferons suppress influenza A virus infection independently of STAT activation by triggering cell death

Wiktor Prus[1], Frederic Grabowski[1], Paulina Koza[1], Zbigniew Korwek[1], Maciej Czerkies[1], Marek Kochańczyk[1], Tomasz Lipniacki[1,2]*

[1] Department of Biosystems and Soft Matter, Institute of Fundamental Technological Research, Polish Academy of Sciences, Warsaw, Poland.

[2] Department of Statistics, Rice University, Houston, TX, USA.

*Corresponding author (e-mail: tlipnia@ippt.pan.pl).

Type III interferons (IFN-λ1–λ4) are known to limit influenza virus infections *in vivo* and are non-redundant to type I interferons (IFN-α and IFN-β). Here, we demonstrated *in vitro* that type III interferons limit infection with influenza A virus (IAV) independently of STAT1 and STAT2 activation. Despite the fact that the knockout of the IFN-λ receptor (subunit IFNLR1), compared to the knockout of the IFN-β receptor (subunit IFNAR1), is associated with higher levels of STAT1/2 phosphorylation during infection, it results in a greater proportion of IAV-infected cells and higher viral RNA and protein levels. We showed that the ratio of dying to infected cells is lower in IFNLR1-deficient cells compared to wild-type cells suggesting that type III interferons limit the spread of IAV by promoting the death of IAV-infected cells. In contrast, type I interferons induce a stronger accumulation of proteins coded by interferon-stimulated genes, and correspondingly suppress IAV spread more effectively than type III interferons when provided prior to infection. Overall, our results suggest an additional non-transcriptional role of type III interferons in the control of viral infections.

Keywords: innate immunity / cell signaling / interferons / respiratory viruses / cell death

Key points:

- IFNAR1 deficiency leads to a significant reduction of STAT1/2 activation in cell populations infected with IAV and a small decrease in IAV proliferation.
- IFNLR1 deficiency leads to a small reduction of STAT1/2 activation in cell populations infected with IAV and a significant increase in IAV proliferation.
- IFN-λ controls the proliferation of IAV (but not RSV) independently of STAT1/2 signaling.
- IFN-λ signaling increases the ratio of the dead to the infected cells, likely by promoting death in IAV-infected cells.

Introduction

The discovery of type III interferons significantly expanded our awareness of the complexity of anti-viral mechanisms in innate immunity (Kotenko *et al*, 2003; Sheppard *et al*, 2003). This relatively novel cytokine family, consisting of interferons λ1, λ2, λ3, and λ4, was initially believed to be mostly supplementary or even redundant to a much better described and understood family of type I interferons (represented importantly by interferons α and β, but also including several others). This was due to similarities between both cytokine families in the mechanisms of their production, recognition, activation of signaling pathways and downstream expression of target genes. The production of cytokines from both families is triggered by recognition of pathogen particles by the same pathogen recognition receptors and is dependent on activation of transcription factors NF-κB and IRF3/7 (Osterlund *et al*, 2007). Type I and type III interferons bind to their cognate receptors, IFNAR1/2 and IFNLR1/IL10R2, respectively, to activate the JAK/STAT pathway, which mediates phosphorylation of STAT1 and STAT2 (collectively referred to as STAT1/2) (Mesev *et al*, 2019). These two transcription factors form a complex with IRF9 and initiate expression of the so-called interferon-stimulated genes (ISGs), which allow the cell to enter a state of increased viral resistance and help activate adaptive immune responses (Schoggins, 2019). These common characteristics of type I and III interferons are generally not shared by type II interferon, IFN-γ, which exhibits a distinct immunomodulatory mode of action and is secreted mostly by specialized immune cells (Schoenborn & Wilson, 2007).

Despite their similarities, accumulating *in vivo* evidence suggests that the roles of type I and III interferons in response to viral infections are partially divergent, with IFN-λ playing a significant role in containing influenza A virus (IAV) infections. In animal studies, Galani *et al*, 2017 demonstrated that IFN-λ suppresses the initial viral spread, ensuring optimal viral clearance, while, in the case of high-dose infections, type I interferons are activated later to enhance antiviral and pro-inflammatory responses. Accordingly, IFNLR1-deficient mice display enhanced type I IFN production and lethality. Klinkhammer *et al*, 2018 showed that in the upper airways IFN-λ but not type I interferons confer long-lasting antiviral protection against influenza virus transmission. A more significant role of type III interferons compared to type I interferons was also observed in mouse models for other viruses, including rotavirus (Pott *et al*, 2011) and norovirus (Nice *et al*, 2015).

The non-redundant and significant role of IFN-λ is puzzling. Despite single reports of type III interferons uniquely inducing certain genes in specific cell lines: *Mmp7*, *Serpinb1a*, and *Csprs* in mouse IEC cells by IFN-λ1 (Selvakumar *et al*, 2017); or *CXCL10, CXCL11, IFIT3, IFI30*, and *TDRD7* in HECV cells also by IFN-λ1 (Caine *et al*, 2019), transcriptome profiling

studies have established that the type I and type III signatures are overlapping, and the ISGs induced by type III IFNs are a subset of those induced by type I IFNs (Lazear *et al*, 2019 and references therein). The major difference is in kinetics and magnitude of expression of genes stimulated by type I and III interferons – strong and rapid in the first group, weaker but more sustained in the second group. Wilder *et al*, 2023 showed (in murine MLE-12 lung epithelial cells) that after 4 h, IFN-β induces over 300 genes, 2.3 times as many as induced by IFN-λ3; however, at 24 h many genes showed a slightly higher induction after IFN-λ3. In their review, Lazear *et al*, 2019 characterize type I *versus* type III interferons as having respectively high/low potency, rapid/slower kinetics, being inflammatory/less inflammatory, systemic/restricted by anatomic barriers. Observations indicate that the expression of IFNLR is generally limited to epithelial surfaces of the airways, gut, liver, urinary tract and the blood–brain barrier, being especially high in the airway epithelium, which contrasts with a much more ubiquitous expression of IFNAR (Lazear *et al*, 2015; Wack *et al*, 2015). Such localized expression of IFNLR predisposes type III interferons to play a major role in combating infections with respiratory viruses. Thus to some extent the distinct role of type III interferons observed in animal models can be attributed to differences in their expression and the expression of their cognate receptor.

In this study, we show that IFN-λ plays a distinct and significant role in limiting infection with IAV, but not with respiratory syncytial virus (RSV), in respiratory epithelial cells *in vitro*. As expected, we observed that prestimulation with IFN-β leads to stronger accumulation of ISGs than prestimulation with IFN-λ1, resulting in a stronger inhibition of both IAV and RSV proliferation. Upon viral infection, phosphorylation of STAT1/2 is dramatically reduced in IFNAR1-deficient but not in IFNLR1-deficient cells, whereas, surprisingly, proliferation of IAV (but not of RSV) is better facilitated by the deficiency of IFNLR1 compared to the deficiency of IFNAR1. Since IFNLR1 has no ligands other than type III interferons (Peterson *et al*, 2019), this indicates that IFN-λ confers protection against IAV through mechanisms beyond JAK/STAT signaling. We observed that the ratio of infected to dead cells is higher in populations of IFNLR1-deficient cells compared to wild-type (WT) cells, indicating that IFN-λ may play a role in promoting the death of infected cells, thereby limiting virus spread.

Results

Stimulation with IFN-β elicits stronger STAT1/2 response and ISG accumulation compared to stimulation with IFN-λ1

Type III interferons are relatively weak inducers of STAT signaling in A549 cells. As shown in Figs. 1A and 1B, stimulation with IFN-λ1 (at its saturation concentration of 50 ng/ml) results

in lower levels of phosphorylated STAT1/2 (p-STAT1/2) after 1 h, after intermediate times (2 and 6 h), and after longer times (24 and 48 h), compared to stimulation with IFN-β (also at its saturation concentration of 1000 U/ml; saturation concentrations for IFN-λ1 and IFN-β were determined in Fig. S1; all replicates of Western blots used in this study are shown in supplementary Source Data S1). Consequently, stimulation with IFN-λ1 compared to IFN-β leads to a lower accumulation of STAT1, STAT2, and three important ISG-coded proteins: RIG-I, PKR, and OAS1 (Figs. 1A and 1B). Similarly, mRNA levels are significantly lower after stimulation with IFN-λ1 compared to IFN-β for 15 out of 16 analyzed ISGs important in the regulation of the innate immune response (Fig. 1C).

Prestimulation with IFN-β inhibits virus proliferation more markedly than prestimulation with IFN-λ1

In our previous study, we have demonstrated that a 24-hour prestimulation with IFN-β reduces IAV RNA count by approximately 300-fold and RSV RNA count by about 5–10-fold (Czerkies *et al*, 2022, Fig 2A and 2B therein). Consistent with the weaker activation of ISGs by IFN-λ1, we have found that a prestimulation with IFN-λ1 has a lesser effect; it reduces IAV RNA count by about 5–10-fold, while the reduction for RSV RNA is insignificant (Czerkies *et al*, 2022, Figs. 2A and 2B therein). The effect is similar at multiplicities of infection (MOI) of 0.1 and 1. The difference between IFN-β and IFN-λ1 is also evident in the number of cells infected with IAV: the prestimulation with IFN-β leads to an about 15-fold reduction in the infected cell count, whereas the prestimulation IFN-λ1 leads to an about 4-fold reduction (Czerkies *et al*, 2022, Fig. 4 therein).

Here, we confirm the more substantial effect of prestimulation with IFN-β compared to IFN-λ1 (for infections with either IAV or RSV) by Western blotting. In the case of an infection with IAV (Figs. 2A and 2B), a 24-hour prestimulation with IFN-β (when compared to both mock and IFN-λ1) leads to significantly higher levels of p-STAT1/2, and, consequently, to higher accumulation of STAT1/2 and ISGs observed at 24 and 48 h post infection (p.i.). This results in drastically lower IAV nucleoprotein (NP) levels, below the detection threshold for all combinations of the MOI and time p.i. In the case of an infection with RSV (Figs. 2C and 2D), p-STAT1/2 levels (at 24 and 48 h p.i.) are similar for non-prestimulated and IFN-λ1- or IFN-β-prestimulated cells, indicating that a sufficient amount of IFN-β is produced during infection to trigger STAT1/2 phosphorylation. However, the early accumulation of ISGs, observed in Figs. 1A and 1B after IFN-β prestimulation, resulted in an about 10-fold reduction of RSV fusion (F) protein levels (compared to non-prestimulated cells), not observed in the case of IFN-λ1 prestimulation (Figs. 2C and 2D).

In summary, we have shown that stimulation with IFN-β, compared to IFN-λ1, leads to a higher level of p-STAT1/2, higher expression of ISGs, and, consequently, when applied before viral infection, more effectively reduces virus spread.

IFNLR1 knockout markedly promotes IAV spread while modestly influencing STAT1/2 signaling

In previous experimental protocols, cells responded to a specific interferon provided during prestimulation and, at later stages of the infection, to type I and type III interferons secreted by infected cells. To disentangle the effect of a single type of interferon during viral infection we employed A549 knock-out cell lines: IFNAR1 KO, IFNLR1 KO, and IFNAR1 & IFNLR1 double KO (further referred to as DKO). We found that despite the fact that in IFNLR1 KO cells the levels of p-STAT1/2, STAT1/2 and ISG are significantly higher ($p < 0.01$) than in IFNAR1 KO cells at 24 and 48 h p.i., accumulation of IAV NP in IFNLR1 KO cells is also significantly stronger compared to IFNAR1 KO and WT cells (Figs. 3A and 3B). IFNAR1 deficiency does not lead to a significant change in IAV NP accumulation when compared to that in WT cells.

This suggests that IFN-λ slows IAV propagation independently of STAT1/2 signaling. This effect is however not observed in the case of infection with RSV, where a significantly weaker accumulation of RSV F protein is observed at 48 h p.i. in IFNLR1 KO cells compared to IFNAR1 KO cells (Figs. 3C and 3D). Given the substantial variability in viral protein levels between experimental replicates, Figs. 3B and 3D present the quantification of eight replicates for IAV and seven replicates for RSV (two from our earlier study, Czerkies *et al*, 2022, and the remaining performed for the current study). Full quantifications, including those for mock infections and DKO cells, can be found in Figs. S2 and S3. The increased spread of IAV in IFNLR1 KO cells, compared to WT cells, is also reflected at the IAV RNA level. Digital PCR measurements (Fig. S4) indicate approximately 3-fold higher accumulation of IAV RNA in IFNLR1 KO cells compared to WT cells (for MOIs of 0.01 and 0.1; 24 to 96 h p.i.), in good agreement with the Western blot results.

Finally, higher levels of IAV mRNA and NP protein observed in IFNLR1 KO cells (but not in IFNAR1 KO cells) with respect to WT cells correlate with a higher fraction of infected cells observed in immunostaining images, shown in Fig. 4A and 4C. We note that p-STAT1 in IFNAR1 KO is almost entirely absent, while p-STAT1 in IFNLR1 KO is not distinguishable from that in WT. Overall, we showed that IFNLR1 deficiency increases IAV NP, IAV RNA, and the fraction of infected cells (with respect to WT), without substantially changing p-STAT1/2 levels and accumulation of ISG-encoded proteins.

Functions of IFN-λ extend beyond induction of ISGs

As shown in the previous section, during IAV infection, lack of IFNLR1 does not significantly hinder the production of the considered ISG-encoded proteins but leads to significantly higher levels of viral RNA, viral proteins, and a greater fraction of infected cells. To exclude the effect of ISG production resulting from IFNLR1 activation, we performed an immunostaining experiment comparing the fraction of IAV-positive cells in WT and IFNLR1 KO cell populations. We prestimulated the cells with 100 U/ml IFN-β for 24 hours before infection with IAV (MOI = 1) and lysed 24 h p.i. (Fig. 4B and 4D). We used a high MOI and a lower IFN-β concentration, because IFN-β prestimulation substantially inhibits IAV spread. We observed that the fraction of infected cells was about 6-fold higher in IFNLR1 KO cells compared to WT cells. This implies that IFN-λ signaling suppresses IAV spread even more effectively when expression of ISGs is already ensured by prior IFN-β prestimulation.

In summary, we demonstrated that IFN-λ signaling hinders viral spread during an infection with IAV (but not with RSV), and this effect is independent of its regulation of expression of ISGs. In the following sections, we argue that IFN-λ signaling is linked to cell death (without distinguishing between apoptosis, pyroptosis, or other cell death types), which is crucial for eliminating infected cells.

Measuring an increase in the cell death rate

We postulate that IAV-infected IFNLR1 KO cells are more resistant to cell death compared to WT cells, allowing for faster virus proliferation. The natural inclination is to compare the number of cell deaths in IFNLR1 KO and WT cell populations infected with IAV. However, a change in the cell death rate affects the total number of infected cells, rendering a direct comparison impossible. Instead, the ratio of cell death events to the number of infected cells is a much more reliable indicator of an increased cell death rate. We clarify this by adapting the susceptible, infected, removed (SIR) model (Eqs. 1–3) to represent viral infection of the cell population, interpreting the removed cells (R) as dead. The kinetics are given by the following equations:

$$S' = -\beta\, I\, S, \tag{1}$$

$$I' = \beta\, I\, S - \lambda\, I, \tag{2}$$

$$R' = \lambda\, I, \tag{3}$$

where ' denotes differentiation with respect to time, β denotes the infection rate, and λ denotes the death rate. In Fig. 5, we show time trajectories of observables R, I, and their ratios for varied values of parameters β and λ for an MOI of 0.1 (see Fig. S5 for MOIs of 0.01

and 0.3). The fraction of dead cells R can increase with λ (at early times) or decrease with λ (at later times), and is generally not monotonic with respect to this parameter (Fig. 5A). This occurs because, at higher λ, the infection progresses more slowly, leading to an overall lower fraction of infected cells (Fig. 5B). However, since the fraction of infected cells (I) is also strongly affected by the infection rate β (Fig. 5C), it cannot be used alone to distinguish between a decrease in mortality and an increase in infectivity. In contrast, the ratio R / I changes strongly and monotonically with λ (Fig. 5D), but weakly and not monotonically with β (Fig. 5E).

In summary, a simultaneous increase in the virus-infected cell fraction (I) and a decrease in the ratio of dead to virus-infected cells (R / I) indicates a decrease in the death rate λ. An important detail is that when experimentally measuring the proportion of infected cells (by immunostaining) or viral proteins or RNA produced by infected cells (by digital PCR or Western blot), we account for live infected cells but also some already dead infected cells. Fortunately, the monotonicity of the ratio R / I with respect to λ implies monotonicity of the ratio $R/(I + \alpha R)$ for any $\alpha \geq 0$. Furthermore, even when $\alpha = 1$, the ratio $R/(I + R)$ still grows substantially with λ (Fig. 5F).

IFN-λ signaling suppresses viral spread by promoting cell death

In Fig. 6A we show that the ratio of cell deaths to accumulated IAV NP is higher in WT cells than in IFNLR1 KO cells, which is equivalent to showing that the ratio of dying to infected cells is higher in the case of WT than IFNLR1 KO cells. The left column of Fig. 6A presents results from Western blots and shows the ratio of IAV NP between IFNLR1 KO and WT cells at 24 h p.i. and 48 h p.i. The amount of IAV NP increases significantly ($p < 10^{-7}$) in IFNLR1 KO cells, consistent with previous experiments (compare with Fig. 3B), despite the high variability observed between experiments.The right column of Fig. 6A shows the ratio of the fraction of cell deaths (measured by FACS) between IFNLR1 KO and WT cells for the same experimental protocol. On average, the ratios are only slightly higher than 1, indicating that the fraction of dead cells in IFNLR1 KO cell populations is comparable to that in WT cell populations. Since the ratio of viral proteins is higher than the ratio of cell deaths, we may conclude that the overall death rate is higher in WT than in IFNLR1 KO cells ($p < 0.01$).

RSV provides a relevant comparison, as it is known that its NS1 protein effectively blocks cell death, promoting viral spread (Bitko *et al*, 2007). To compare cell death rates during infection with IAV and RSV, we measured fractions of cells displaying propidium iodide signal during 24 and 48 hour long infections. Next, the cells were fixed, and fractions of virus positive cells at 24 and 48 hours were measured based on immunostaining images. In Fig.

6B, we show that cell death fractions for RSV and IAV are similar, but the infected cell fraction is much higher for infection with RSV than for infection with IAV. Consequently, this indicates a higher death rate for IAV infections compared to RSV infections ($p < 0.01$). The effect is observed for both WT and IFNLR1 KO cells. This supports our reasoning that an inhibition of cell death can be manifested by an increase of the fraction of infected cells rather than a decrease in the fraction of dead cells, suggesting that IFN-λ signaling suppresses viral spread by promoting cell death.

Discussion

Using WT, IFNLR1 KO, IFNAR1 KO, and IFNLR1–IFNAR1 DKO A549 cells, we demonstrated divergent roles of type I and type III interferons in control of IAV and RSV proliferation. (**1**) We showed that (pre)stimulation with IFN-β leads to a strong increase of p-STAT1/2 and STAT1/2 levels, high accumulation of ISGs, and, through those mechanisms, a pronounced reduction of proliferation of IAV as well as RSV. Prestimulation with IFN-λ (compared to IFN-β) results in lower levels of p-STAT1/2 and STAT1/2, lower accumulation of ISGs, and only moderately reduces proliferation of IAV, and does not reduce proliferation of RSV. (**2**) Next, we showed that in IAV- or RSV-infected IFNAR1 KO cells, p-STAT1/2, STAT1/2 and ISG levels are pronouncedly reduced with respect to those in WT and IFNLR1 KO cells. However, IAV proliferates significantly faster in IFNLR1 KO cells than in WT or IFNAR1 KO cells. This indicates that IFN-λ suppresses IAV proliferation independently to STAT signaling. We note the possibility that IFNLR1 inhibits IAV proliferation independently of type III interferons, however mouse studies indicate that type III interferon deficiency has the same consequences as IFNLR1 deficiency during infections with norovirus, reovirus, and influenza virus (Peterson *et al*, 2019). The faster viral propagation in IFNLR1 KO cells is not observed for RSV. (**3**) Finally, we showed that absence of IFN-λ signaling significantly increases the level of IAV protein and the fraction of infected cells, without an increase in the fraction of dead cells. With the help of a simple mathematical model we interpret this observation as the ability of IFN-λ to promote early death in cells infected with IAV. Additionally, we showed that for infection with IAV, the ratio of dead to infected cells is higher than for infection with RSV. This is in line with earlier observations that NS proteins of RSV very effectively suppress cell death in infected cells, promoting virus proliferation (Bitko *et al*, 2007). This could explain why the effect of IFN-λ on RSV spread appears negligible.

Although divergent roles of type I and type III interferons have been highlighted in numerous studies, reports of a non-transcriptional role, especially proapoptotic (or propyroptotic), of IFN-λ are scarce. In two studies not related to infections, it was shown that in intestinal cells type III interferons (compared to type I interferons) are a more potent

inducers of apoptosis (Li *et al*, 2008) and pyroptosis (preprint: Sposito *et al*, 2022). Broggi et al (Broggi *et al*, 2017), in a study not directly related to infections, showed that IFN-λ regulates functions of neutrophils (known to have high expression of IFNLR) independently of transcription, and that treatment with IFN-λ induced in these cells a reduction in the phosphorylation of AKT at Ser473 and Thr308, which could make these cells more prone to cell death. Earlier, Denisova et al (Denisova *et al*, 2014) showed that inhibiting AKT suppresses proliferation of IAV in A549 cells. Major et al (Major *et al*, 2020) found that IFN signaling (especially IFN-λ) hampers lung repair by inducing p53 which activates antiproliferative and cell death pathways. Transcriptional regulation of p53 by interferons was also demonstrated in an earlier study by Takaoka et al (Takaoka *et al*, 2003). In the context of viral infections, a straightforward demonstration that IFN-λ increases the cell death rate is challenging because a higher cell death rate does not necessarily result in a greater fraction of dead cells, as it also suppresses viral propagation. We suspect that this may partially explain why this phenomenon was not reported earlier.

Our findings confirm that the role of IFN-β is to promote an antiviral state in not yet infected bystander cells, which increases their resistance to infection and/or slows down virus replication once they are infected. In terms of the SIR model, the effect of IFN-β can be seen as a reduction of the infection rate coefficient β, see Eq. (2). The role of IFN-λ (apart from STAT signaling) would be to promote cell death, and thus removal of infected cells. In the SIR model, this corresponds to an increase of the death rate coefficient λ, see also Eq. (2). In this picture, type III interferons are more universal than type I interferons, being able to both induce some STAT signaling and trigger cell death. Finally, it should be stressed that our data does not exclude the possibility that IFN-λ triggers cell death using ISGs that are accumulated (mostly) due to IFN-β signaling. This is in line with the observation that the effect of IFNLR1 deficiency is the strongest when cells are already prestimulated with IFN-β, and our earlier study (Czerkies *et al*, 2018) which showed that the death rate after poly(I:C) stimulation is much higher in IFN-β-prestimulated cells.

Methods

Cell lines and cultures. The A549, HEK-293T, HeLa and MDCK cell lines were purchased from the ATCC. A549 cells were cultured in F-12K basal medium supplemented with 10% fetal bovine serum (FBS) and a penicillin-streptomycin antibiotic solution. MDCK, HeLa cells and HEK-293T cells were maintained in Dulbecco's modified Eagle's medium (DMEM) supplemented with 10% FBS and a penicillin-streptomycin antibiotic solution. All cell lines were cultured under standard conditions (37°C with 5% CO_2) and kept in monolayers up to 90% confluence. The IFNAR1, IFNLR1, and IFNAR1-IFNLR1 knockouts based on the A549

cell line were developed using the CRISPR lentivirus system (Abm). The detailed procedure for obtaining these cell lines have been described in (Czerkies *et al*, 2022, see Methods section and Supplementary Figure S3 therein).

Virus amplification,isolation and quantification has been performed as described before in Czerkies *et al*, 2022.

Compounds and stimulation protocols. Human IFN-β1A and IFN-λ1 were purchased from Thermo Fisher Scientific (catalog numbers PHC4244 and 34-8298-64, respectively) and prepared according to the manufacturer's instructions. For cell stimulation, interferons were further diluted to the desired concentrations in F-12K medium supplemented with 2% FBS, to prevent the inhibition of viral attachment and entry by serum proteins.

Interferon–virus experiments have been performed as described previously in Czerkies *et al*, 2022: the cell culture media were exchanged for interferon-containing or control media at time zero and were not removed afterward until the end of the experiment. Appropriately diluted virus was added in small volumes (less than 10 μL) directly into the wells. The even distribution of virus across the cell population was aided by the intermittent rocking of the plate for 2 h.

Antibodies. (i) Antibodies for Western blotting. Primary antibodies for Western blotting were anti-phospho-STAT1 (Tyr701) (clone 58D6) (catalog number 9167; Cell Signaling Technologies) (1:1,000), anti-phospho-STAT2 (Tyr690) (clone D3P2P) (catalog number 88410; Cell Signaling Technologies) (1:1,000), anti-RIG-I (clone D14G6) (catalog number 3743; Cell Signaling Technologies) (1:1,000), anti-STAT1 (catalog number 610116; BD Biosciences) (1:1,000), anti-STAT2 (catalog number PAF-ST2; R&D Systems) (1:1,000), anti-PKR (clone B-10) (catalog number sc-6282; Santa Cruz Biotechnology) (1:1,000), anti-OAS1 (clone F-3) (catalog number sc-374656; Santa Cruz Biotechnology) (1:1,000), anti-influenza A virus nucleoprotein (clone C43) (catalog number ab128193; Abcam) (1:1,000), anti-respiratory syncytial virus (clone 2F7) (catalog number ab43812; Abcam) (1:1,000), and hFAB rhodamine anti-glyceraldehyde-3-phosphate dehydrogenase (GAPDH) (catalog number 12004168; Bio-Rad) (1:10,000).

Secondary antibodies for Western blotting were DyLight 800 4× PEG-conjugated goat anti-rabbit IgG(H+L) (catalog number SA5-35571; Thermo Fisher Scientific) (1:10,000), DyLight 800 4× PEG-conjugated goat anti-mouse IgG(H+L) (catalog number SA5-35521; Thermo Fisher Scientific) (1:10,000), StarBright Blue 700-conjugated goat anti-mouse IgG (catalog number 12004159; Bio-Rad) (1:10,000), and horseradish peroxidase (HRP)-conjugated rabbit anti-goat immunoglobulins (catalog number P0449; Agilent) (1:10,000).

(ii) Antibodies for immunostaining. Primary antibodies for immunostaining were anti-phospho-STAT1 (Tyr701) (clone 58D6) (catalog number 9167; Cell Signaling Technologies) (1:1,000), anti-respiratory syncytial virus (catalog number ab20745; Abcam) (1:1,000), anti-influenza A virus (catalog number ab20841; Abcam) (1:1,000), anti-influenza A virus nucleoprotein (clone C43) (catalog number ab128193; Abcam) (1:1,000), and anti-human interferon beta (catalog number MAB8142; R&D Systems).

Secondary antibodies for immunostaining were Alexa Fluor 488-conjugated donkey anti-rabbit IgG(H+L) (catalog number A-21206; Thermo Fisher Scientific) (1:1,000), Alexa Fluor 555-conjugated donkey anti-mouse IgG(H+L) (catalog number A-31570; Thermo Fisher Scientific) (1:1,000), and Alexa Fluor 633-conjugated donkey anti-goat IgG(H+L) (catalog number A-21082; Thermo Fisher Scientific) (1:1,000).

RNA isolation. For gene expression analysis experiments, cells were seeded on 12- or 24-well plates (Falcon) at a density of, respectively, 1.0×10^5 or 1.5×10^5 cells/well. Upon completed stimulation according to chosen protocol, cells were washed once with PBS and submitted to isolation of total RNA using PureLink RNA Mini Kit (Thermo Fisher Scientific), following manufacturer's instructions: cells were harvested and vortexed in Lysis Buffer with 2-mercaptoethanol and then vortexed again with one volume of 70% ethanol. Upon transferring to the spin cartridge, cellular RNA content was bound to the column, washed with appropriate buffers and eluted, all by centrifugation at 12,000×*g*. Eluted RNA in RNase-free water was used immediately for reverse transcription or stored for later use at −80 °C.

Reverse transcription. RNA concentration and quality was determined by measuring UV absorbance of samples diluted 1:100 in 10 mM Tris-HCl (pH 7.5) at 260 and 280 nm, using the Multiskan GO spectrophotometer (Thermo Fisher Scientific). Independently, RIN index for isolated RNA was checked using Agilent 2100 Bioanalyzer. Around 1 µg of RNA was used as a template for reverse transcription, performed using High-Capacity cDNA Reverse Transcription Kit (Thermo Fisher Scientific). Following manufacturer's protocol, diluted RNA samples were mixed 1:1 with freshly prepared Master Mix containing RT Buffer, RT Random Primers, dNTP Mix, MultiScribe Reverse Transcriptase and RNase Inhibitor. Reaction was performed in Mastercycle Gradient thermal cycler (Eppendorf) under following conditions: 10 min at 25 °C, 120 min at 37 °C, and 5 min at 85 °C.

Real-Time Quantitative PCR. Reaction was performed on a QuantStudio 12K Flex Real-Time PCR system with Array Card block (Life Technologies). In most cases, 750 ng of cDNA from reverse transcription was mixed with reaction Master Mix and loaded onto TaqMan Array Card containing probes and primers for 24 genes (in 2 replicates), including

endogenous reference controls (see Source Data S2). Reaction was conducted using QuantStudio “Standard” protocol, with FAM/ROX chemistry. Upon completion, expression of target genes was analyzed based on absolute Ct quantification or classical ΔΔCt method with QuantStudio 12K Flex software, normalized against GAPDH gene expression.

Digital PCR. For viral RNA copy number measurements, cells were seeded onto 24-well plates at a density of 100,000 cells per well andRNA from virus-infected cell populations was isolated and reverse-transcribed as described above. Then, digitalPCR using QuantStudio3D system (Thermo Fisher Scientific) with TaqMan Vi99990011_po and Vi99990014_po gene expression assays have been performed as described previously in Czerkies *et al*, 2022.

Western blotting has been performed as previously described in Czerkies *et al*, 2022.

Immunostaining has been performed using a modified protocol described previously in Czerkies *et al*, 2022**,** with cells mounted onto microscope slides using Vectashield Antifade Mounting Medium (Vector Labs), instead of Mowiol used in the previous publication.

FACS/Cell death assay. Cell death was measured using annexin V and propidium iodide staining method, according to protocol described previously in Czerkies *et al*, 2018. Cells which are both annexin V- and propidium iodide (PI)-negative were considered viable, annexin V-positive and PI-negative were considered early apoptotic or pyroptotic; PI-positive cells, irrespective of the outcome of annexin V staining, were considered dying or dead.

Live imaging propidium iodide assay. To estimate cell death rates during infection with IAV and RSV, live imaging of PI intracellular accumulation was performed. One day before the experiment, cell nuclei were stained with Hoechst 33342 (Thermo) diluted 1 µg/ml in PBS for 10 minutes at 37°C. After staining, the cells were washed and seeded onto a µClear 96-well microplate at a density of 18,000 cells per well. The following day, the cells were infected with IAV or RSV, and PI was added. Cells were observed for 24 or 48 h, and within these periods fraction of PI positive cells was determined. After 24 or 48 h p.i. cell fixation and immunostaining were performed to estimate the number of infected cells. Imaging was carried out on an Operetta CLS (PerkinElmer) using Harmony software. Images were analyzed using our in-house software, ShuttleTracker (see the Image analysis section below).

Image analysis. Confocal images obtained from immunostaining were analyzed using our in-house software (https://pmbm.ippt.pan.pl/software/shuttletracker). Nuclear outlines were detected based on DAPI staining. Outlines of nuclei that were partially out of frame or mitotic

were excluded from the analysis; outlines of overlapping nuclei were split based on geometric convexity defects when possible. Cells were classified as either virus-negative or virus-positive based on the sum of the intensities of the pixels inside nuclear outlines. Cells were classified as dead/dying based on the intensities of pixels inside nuclear outlines in the PI channel.

Statistical analysis. Western blot quantifications were first normalized by the corresponding reference GAPDH, then by the maximum value (for each protein and replicate separately). Finally, 0.03 was added to each value, as justified in Grabowski *et al*, 2023. For statistical analysis, the resulting values were additionally log-transformed. To account for independent normalization of each experimental replicate, in ANOVA tests we treat replicate ID as an additional factor. This approach ensures that rescaling an individual replicate by a constant factor does not change the result of the statistical test.

In Fig. 1B, the factors in ANOVA were: stimulation agent (IFN-β or IFN-λ), stimulation time (1, 2, 6, 24, 48 h for p-STAT1/2; 24, 48 h for STAT1/2), replicate ID (assuming no interaction with other factors). For each considered protein the significance of the stimulation agent was tested, and the results were corrected using the Benjamini–Hochberg procedure (with 5% false discovery rate). In Figs. 2B and 2D, the factors in ANOVA were: stimulation agent (mock, IFN-β, IFN-λ), stimulation conditions (MOI 0.1 24 h, MOI 0.1 48 h, MOI 1 24 h, MOI 1 48 h), replicate ID (assuming no interaction with other factors). For each considered protein the significance of the stimulation agent was tested, and the results were corrected using the Benjamini–Hochberg procedure (5% false discovery rate). For proteins in which a significant difference was observed, pairwise significance levels between stimulation agents obtained by the Tukey *post-hoc* are reported. In Figs. 3B and 3D, the factors in ANOVA were: cell line (WT, IFNAR1 KO, IFNLR1 KO), stimulation time (24 h, 48 h), replicate ID (assuming no interaction with other factors); with the exception of RSV F in Fig. 3D, where only measurements at 48 h were considered and thus only two factors remain. For each considered protein the significance of the cell line was tested, and the results were corrected using the Benjamini–Hochberg procedure (with 5% false discovery rate). In all cases a significant difference was observed, and pairwise significance levels between cell lines obtained by the Tukey *post-hoc* are reported (for each pair of cell lines).

In Fig. 1C, RT-PCR was similarly analyzed using ANOVA. Data for each mRNA were analyzed independently, with factors: stimulation agent (IFN-β or IFN-λ), stimulation time (6, 10, 24 h), replicate ID (assuming no interaction with other factors). For each mRNA the significance of the stimulation agent was tested, and the results were corrected using the Benjamini-Hochberg procedure (with 5% false discovery rate).

Statistical significance in Figs. 4A and 4B, Fig. S4 was assessed using the Student *t*-test. In Fig. 6A we performed both a Welch *t*-test (unpaired Student *t*-test without assuming equal variances) and Mann–Whitney *U* test, while in Fig. 6B we performed a Student *t*-test and Wilcoxon signed-rank *U* test. All tests assume two-tailed alternatives.

In the case of Fig. 4A, Fig. 6A, Fig. S4, the statistical tests were performed using experimental replicates obtained for two or three time points pooled together; similarly, in Fig. 4A and Fig. S4 two MOI values (0.01 and 0.1) are considered jointly. In these cases our data indicates that the studied relative differences between cell lines do not change over time or with MOI (for the considered time periods and MOIs).

In particular, in Fig. 6A, the left column consists of IAV NP level ratios between IFNLR1 KO and WT cells, where both levels are measured in a single Western blot. The right column consists of ratios between the fraction of dying/dead cells between IFNLR1 KO and WT cells; both fractions are measured in a single FACS experiment. However, ratios from the left column are not paired with ratios from the right column (since the Western blot and FACS measurements were not paired). Thus, we use a (parametric) Welch's *t*-test and a (non-parametric) Mann–Whitney *U* test to compare log ratios from the left column with log ratios from the right column. Data from time points 24 h p.i. and 48 h p.i. are considered jointly.

In Fig. 6B, ratios from the left column (obtained from immunostaining images of fixed cells) and ratios from the right column (obtained from live-cell imaging) are paired, since both types of measurement were performed for the same cell population (for each experimental replicate). For each left–right pair, we can thus compute a ratio-of-ratios. We then perform a (parametric) two-tailed Student *t*-test and a (non-parametric) two-tailed Wilcoxon signed-rank test on log ratio-of-ratios. Data from time points 24 h p.i. and 48 h p.i. and cell lines WT and IFNLR1 KO are considered jointly, since the death rate in IAV is always higher than in RSV (which is equivalent to ratio-of-ratios greater than 1).

Data availability

All Western blots performed for this study are available in supplementary file Source Data S1. Quantifications of Western blots, RT-PCR, digital PCR, FACS, imaging data and codes to generate figures are available in supplementary file Source Data S2. The raw imaging dataset is available at Zenodo (doi: 10.5281/zenodo.13735878).

Author contributions

Conceptualization: Wiktor Prus, Frederic Grabowski, Paulina Koza, Zbigniew Korwek, Maciej Czerkies, Marek Kochańczyk, Tomasz Lipniacki.

Methodology: Wiktor Prus, Paulina Koza, Zbigniew Korwek, Maciej Czerkies.

Formal analysis: Frederic Grabowski.

Investigation: Wiktor Prus, Paulina Koza, Zbigniew Korwek, Maciej Czerkies.

Data curation: Frederic Grabowski, Marek Kochańczyk.

Writing – original draft: Wiktor Prus, Frederic Grabowski, Zbigniew Korwek, Maciej Czerkies, Marek Kochańczyk, Tomasz Lipniacki.

Writing – review & editing: Wiktor Prus, Frederic Grabowski, Paulina Koza, Zbigniew Korwek, Maciej Czerkies, Marek Kochańczyk, Tomasz Lipniacki.

Visualization: Frederic Grabowski.

Supervision: Marek Kochańczyk, Tomasz Lipniacki.

Funding acquisition: Tomasz Lipniacki.

Disclosure and competing interest statement

The authors declare no competing interests.

Acknowledgements

This study was funded by the Norwegian Financial Mechanism GRIEG-1 grant (operated by the National Science Centre, Poland) 2019/34/H/NZ6/00699 (TL) and the National Science Centre Poland grant 2023/51/B/NZ6/02951 (TL). The funders had no role in study design, data collection and analysis, decision to publish, or preparation of the manuscript.

References

Bitko V, Shulyayeva O, Mazumder B, Musiyenko A, Ramaswamy M, Look DC & Barik S (2007) Nonstructural proteins of respiratory syncytial virus suppress premature apoptosis by an NF-kappaB-dependent, interferon-independent mechanism and facilitate virus growth. *J Virol* 81: 1786–1795

Broggi A, Tan Y, Granucci F & Zanoni I (2017) IFN-λ suppresses intestinal inflammation by non-translational regulation of neutrophil function. *Nat Immunol* 18: 1084–1093

Caine EA, Scheaffer SM, Arora N, Zaitsev K, Artyomov MN, Coyne CB, Moley KH & Diamond MS (2019) Interferon lambda protects the female reproductive tract against Zika virus infection. *Nat Commun* 10: 280

Czerkies M, Kochańczyk M, Korwek Z, Prus W & Lipniacki T (2022) Respiratory syncytial virus protects bystander cells against influenza A virus infection by triggering secretion of type I and type III Interferons. *J Virol* 96: e0134122

Czerkies M, Korwek Z, Prus W, Kochańczyk M, Jaruszewicz-Błońska J, Tudelska K, Błoński S, Kimmel M, Brasier AR & Lipniacki T (2018) Cell fate in antiviral response arises in the crosstalk of IRF, NF-κB and JAK/STAT pathways. *Nat Commun* 9: 493

Denisova OV, Söderholm S, Virtanen S, Von Schantz C, Bychkov D, Vashchinkina E, Desloovere J, Tynell J, Ikonen N, Theisen LL, *et al* (2014) Akt Inhibitor MK2206 Prevents Influenza pH1N1 Virus Infection In Vitro. *Antimicrob Agents Chemother* 58: 3689–3696

Galani IE, Triantafyllia V, Eleminiadou E-E, Koltsida O, Stavropoulos A, Manioudaki M, Thanos D, Doyle SE, Kotenko SV, Thanopoulou K, *et al* (2017) Interferon-λ Mediates Non-redundant Front-Line Antiviral Protection against Influenza Virus Infection without Compromising Host Fitness. *Immunity* 46: 875-890.e6

Grabowski F, Kochańczyk M, Korwek Z, Czerkies M, Prus W & Lipniacki T (2023) Antagonism between viral infection and innate immunity at the single-cell level. *PLOS Pathog* 19: e1011597

Klinkhammer J, Schnepf D, Ye L, Schwaderlapp M, Gad HH, Hartmann R, Garcin D, Mahlakõiv T & Staeheli P (2018) IFN-λ prevents influenza virus spread from the upper airways to the lungs and limits virus transmission. *eLife* 7: e33354

Kotenko SV, Gallagher G, Baurin VV, Lewis-Antes A, Shen M, Shah NK, Langer JA, Sheikh F, Dickensheets H & Donnelly RP (2003) IFN-lambdas mediate antiviral protection through a distinct class II cytokine receptor complex. *Nat Immunol* 4: 69–77

Lazear HM, Nice TJ & Diamond MS (2015) Interferon-λ: Immune Functions at Barrier Surfaces and Beyond. *Immunity* 43: 15–28

Lazear HM, Schoggins JW & Diamond MS (2019) Shared and Distinct Functions of Type I and Type III Interferons. *Immunity* 50: 907–923

Li W, Lewis-Antes A, Huang J, Balan M & Kotenko SV (2008) Regulation of apoptosis by type III interferons. *Cell Prolif* 41: 960–979

Major J, Crotta S, Llorian M, McCabe TM, Gad HH, Priestnall SL, Hartmann R & Wack A (2020) Type I and III interferons disrupt lung epithelial repair during recovery from viral infection. *Science* 369: 712–717

Mesev EV, LeDesma RA & Ploss A (2019) Decoding type I and III interferon signalling during viral infection. *Nat Microbiol* 4: 914–924

Nice TJ, Baldridge MT, McCune BT, Norman JM, Lazear HM, Artyomov M, Diamond MS & Virgin HW (2015) Interferon-λ cures persistent murine norovirus infection in the absence of adaptive immunity. *Science* 347: 269–273

Osterlund PI, Pietilä TE, Veckman V, Kotenko SV & Julkunen I (2007) IFN regulatory factor family members differentially regulate the expression of type III IFN (IFN-lambda) genes. *J Immunol Baltim Md 1950* 179: 3434–3442

Peterson ST, Kennedy EA, Brigleb PH, Taylor GM, Urbanek K, Bricker TL, Lee S, Shin H, Dermody TS, Boon ACM, *et al* (2019) Disruption of Type III Interferon (IFN) Genes Ifnl2 and Ifnl3 Recapitulates Loss of the Type III IFN Receptor in the Mucosal Antiviral Response. *J Virol* 93: 10.1128/jvi.01073-19

Pott J, Mahlakõiv T, Mordstein M, Duerr CU, Michiels T, Stockinger S, Staeheli P & Hornef MW (2011) IFN-λ determines the intestinal epithelial antiviral host defense. *Proc Natl Acad Sci* 108: 7944–7949

Schoenborn JR & Wilson CB (2007) Regulation of interferon-gamma during innate and adaptive immune responses. *Adv Immunol* 96: 41–101

Schoggins JW (2019) Interferon-Stimulated Genes: What Do They All Do? *Annu Rev Virol* 6: 567–584

Selvakumar TA, Bhushal S, Kalinke U, Wirth D, Hauser H, Köster M & Hornef MW (2017) Identification of a Predominantly Interferon-λ-Induced Transcriptional Profile in Murine Intestinal Epithelial Cells. *Front Immunol* 8: 1302

Sheppard P, Kindsvogel W, Xu W, Henderson K, Schlutsmeyer S, Whitmore TE, Kuestner R, Garrigues U, Birks C, Roraback J, *et al* (2003) IL-28, IL-29 and their class II cytokine receptor IL-28R. *Nat Immunol* 4: 63–68

Sposito B, Mambu J, Gwilt KB, Spinelli L, Andreeva N, Galland F, Naquet P, Mitsialis V, Thiagarajah JR, Snapper SB, *et al* (2022) Type III interferons induce pyroptosis in gut epithelial cells and delay tissue restitution upon acute intestinal injury. 2022.03.04.482997 doi:10.1101/2022.03.04.482997 [PREPRINT]

Takaoka A, Hayakawa S, Yanai H, Stoiber D, Negishi H, Kikuchi H, Sasaki S, Imai K, Shibue T, Honda K, *et al* (2003) Integration of interferon-α/β signalling to p53 responses in tumour suppression and antiviral defence. *Nature* 424: 516–523

Wack A, Terczyńska-Dyla E & Hartmann R (2015) Guarding the frontiers: the biology of type III interferons. *Nat Immunol* 16: 802–809

Wilder CL, Lefaudeux D, Mathenge R, Kishimoto K, Zuniga Munoz A, Nguyen MA, Meyer AS, Cheng QJ & Hoffmann A (2023) A stimulus-contingent positive feedback loop enables IFN-β dose-dependent activation of pro-inflammatory genes. *Mol Syst Biol* 19: e11294

Figure legends

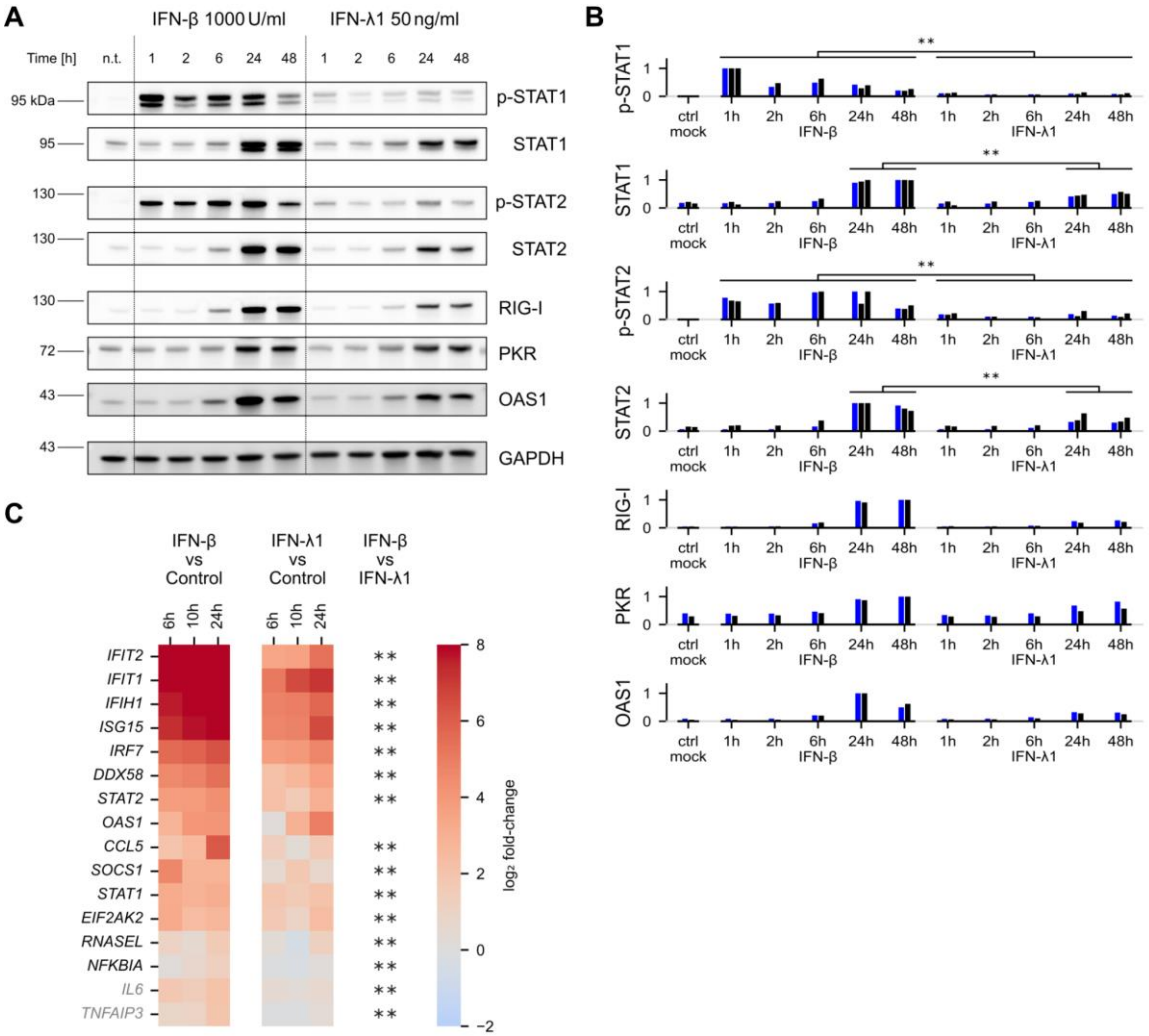

Figure 1. STAT1/2 activation and accumulation of ISGs after stimulation with IFN-β and IFN-λ1.

A A549 cells were stimulated with IFN-β (1000 U/ml) or IFN-λ1 (50 ng/ml) for 1, 2, 6, 24, or 48 h before lysis; p-STAT1, STAT1 phosphorylated at Tyr701; p-STAT2, STAT2 phosphorylated at Tyr690.

B Quantification of two or three experimental replicates (as shown). Blue bars indicate the experimental replicate shown in panel A. Each blot quantification is normalized to the maximum. The significances $p < 0.01$ (**) were determined using multiple ANOVA on log intensities corrected using 5% Benjamini–Hochberg false discovery rate (see Methods for details).

C RT-PCR of common ISGs as well as *IL6* and *TNFAIP3* after 6, 10, and 24 h stimulation with either IFN-β (1000 U/ml) or IFN-λ1 (50 ng/ml). The averaged $\log_2$ difference (based on 3 experimental replicates) with respect to control is shown. Asterisks indicate that expression of a given gene after stimulation with IFN-β is significantly different (higher) than after IFN-λ1 at $p < 0.01$ (**); multiple ANOVA on $\log_2$ differences corrected using 5% Benjamini–Hochberg false discovery rate (see Methods for details).

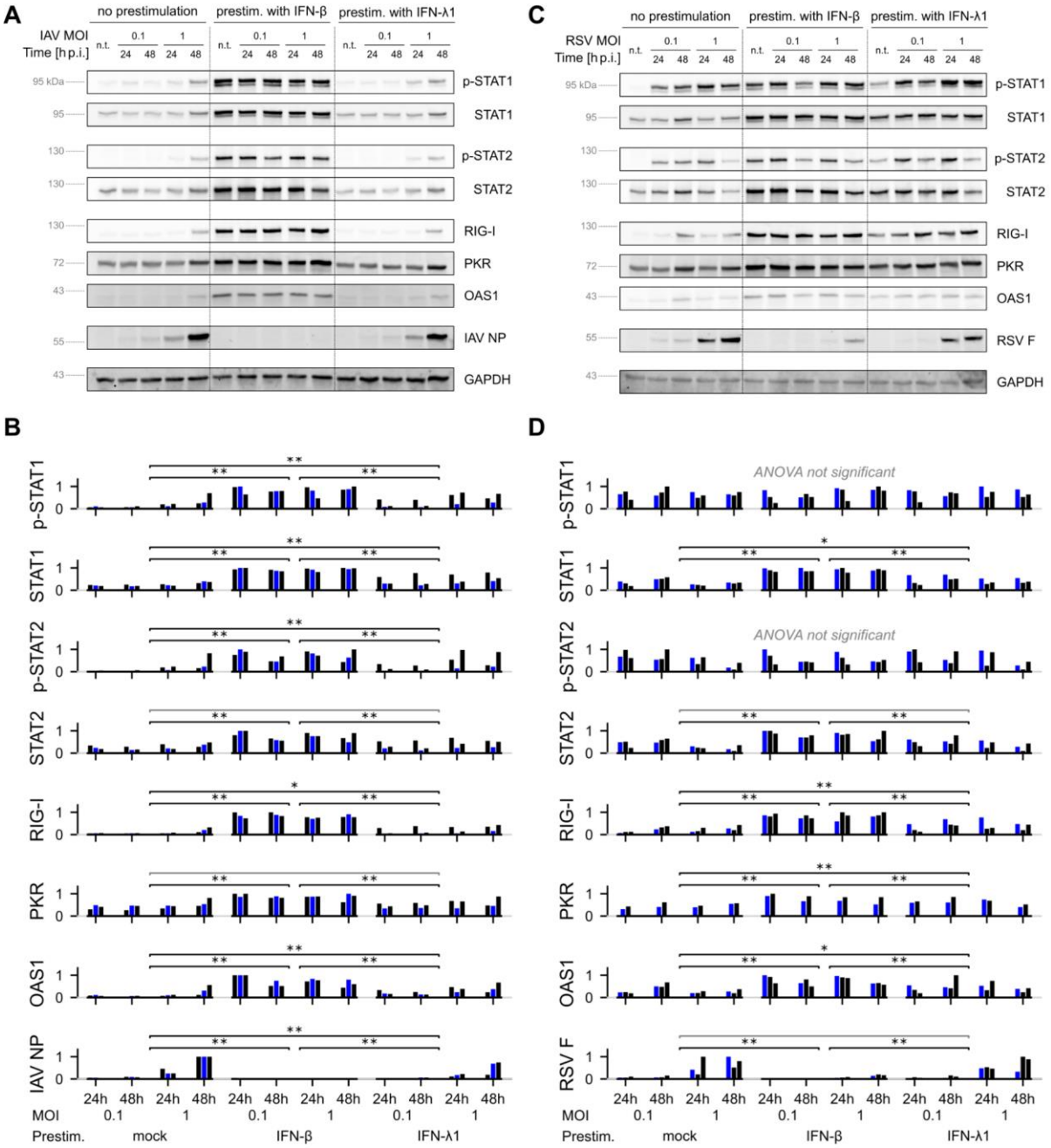
A
no prestimulation
prestim. with IFN-β
prestim. with IFN-λ1
IAV MOI
Time [h p.i.]
n.t.
0.1
1
24
48
95 kDa
p-STAT1
STAT1
p-STAT2
STAT2
RIG-I
PKR
OAS1
IAV NP
GAPDH
C
RSV MOI
RSV F
B
D
ANOVA not significant
MOI
Prestim.
mock
IFN-β
IFN-λ1

593

▲ *(continued from the previous page)*

Figure 2. Effect of the prestimulation with IFN-β and IFN-λ1 on STAT1/2 activation, expression of ISGs, and virus proliferation.

A A549 cells were prestimulated with either IFN-β or IFN-λ1 (or mock) 24 h before infection with IAV at MOIs of 0.1 or 1 and lysed 24 or 48 h post infection (p.i.). Label 'n.t.' denotes cells not treated with a virus.

B Quantification of three replicates of the experiment shown in A. Blue bars indicate the experimental replicate shown in panel A.

C A549 cells were prestimulated with IFN-β or IFN-λ1 (or mock) 24 h before infection with RSV at MOIs of 0.1 or 1 and lysed 24 or 48 h post infection (p.i.). Label 'n.t.' denotes cells not treated with a virus.

D Quantification of three replicates of the experiment shown in C. Blue bars indicate the experimental replicate shown in panel C.

In panels A and C, due to all available 15 lanes being used for probes, the marker lane was omitted. Locations of molecular weight markers were determined based on previous experiments.

In panels B and D, quantification of the bands without infection with IAV or RSV (n.t.) are omitted. Each blot quantification is normalized to the maximum. Differences between prestimulations were determined using multiple ANOVA tests on log intensities, corrected with 5% Benjamini-Hochberg false discovery rate. For proteins with significant differences, Tukey *post-hoc* tests were performed to obtain p values: $p < 0.05$ (*) and $p < 0.01$ (**) (see Methods for details).

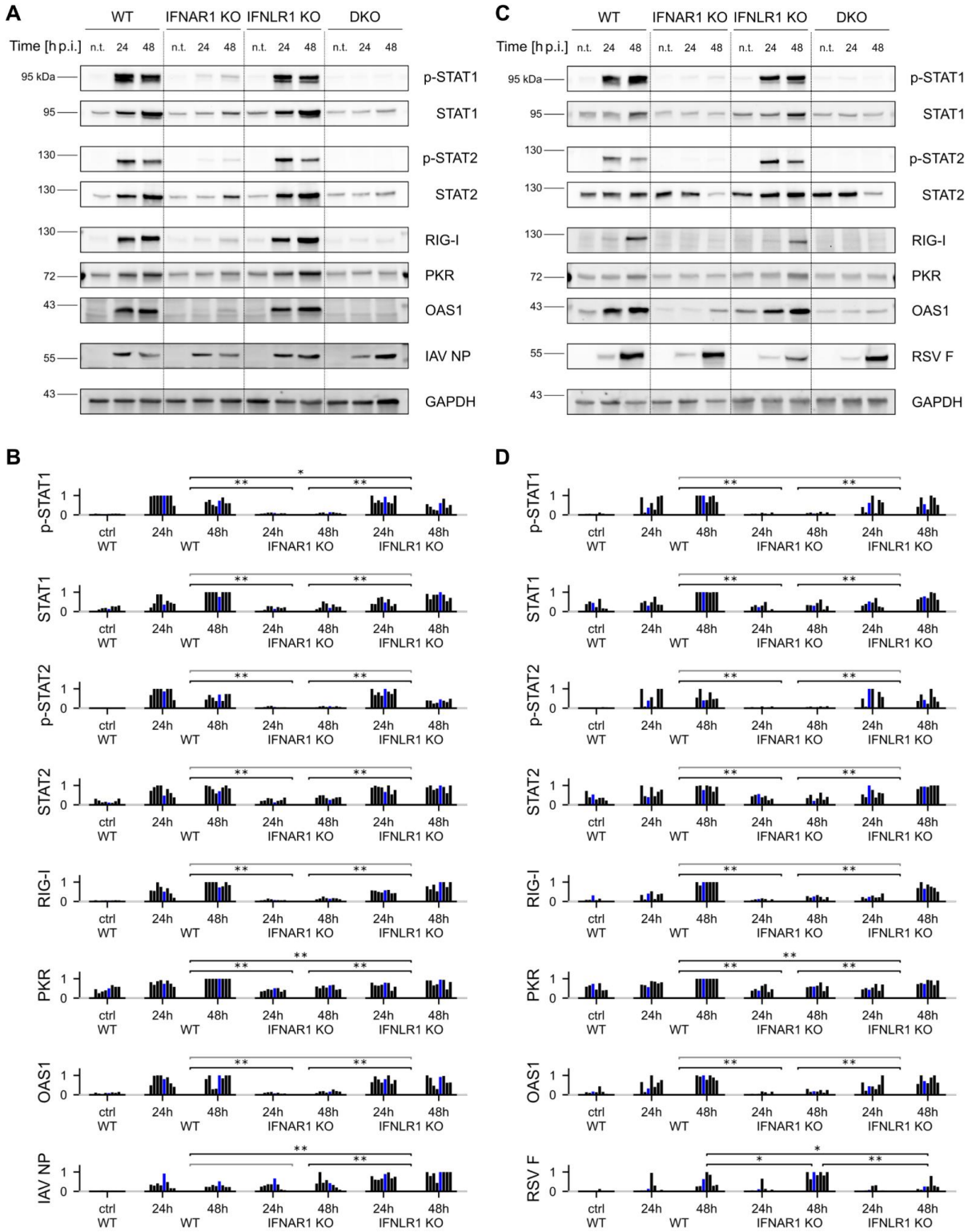
A
WT
IFNAR1 KO
IFNLR1 KO
DKO
Time [h p.i.]
n.t.
24
48
95 kDa
p-STAT1
STAT1
p-STAT2
STAT2
RIG-I
PKR
OAS1
IAV NP
GAPDH
C
RSV F
B
D
ctrl
WT
IFNAR1 KO
IFNLR1 KO

616

▲ *(continued from the previous page)*

Figure 3. Effect of IFNLR1 and IFNAR1 knockout on IAV and RSV proliferation and activation of immune response

A A549 WT, IFNAR1 KO, IFNLR1 KO, and IFNAR1 & IFNLR1 double KO (DKO) cells were infected with IAV at an MOI of 0.1 and lysed 24 or 48 h p.i.

B Quantification of selected bands from blots in panel A and its seven replicates at 48 h Quantification of the shown blot is marked in blue.

C A549 WT, IFNAR1 KO, IFNLR1 KO and DKO cells were infected with RSV at an MOI of 0.1 and lysed 24 or 48 h p.i.

D Quantification of selected bands from blots in panel C and its six replicates at 48 h. Quantification of the shown blot is marked in blue.

In panels B and D, differences between cell lines were determined using multiple ANOVA tests on log intensities, corrected with 5% Benjamini-Hochberg false discovery rate. For proteins with significant differences, Tukey *post-hoc* tests were performed to obtain *p* values: $p < 0.05$ (*) and $p < 0.01$ (**) (see Methods for details). Each blot quantification is normalized to the maximum. The quantification of all cell lines (including DKO) from blots in A and C is shown in Figs. S2 and S3.

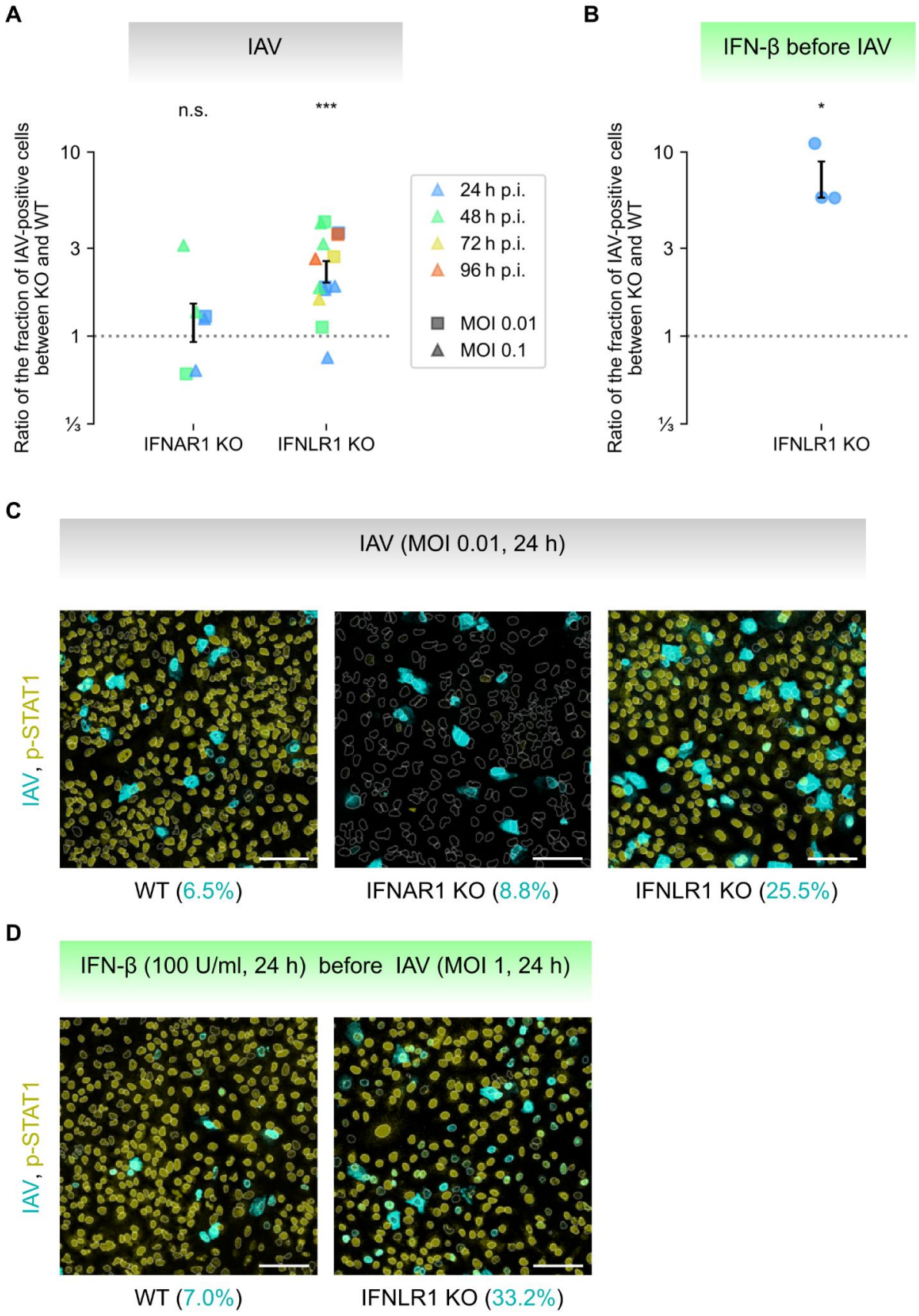
A
IAV
n.s.
***
Ratio of the fraction of IAV-positive cells between KO and WT
10
3
1
⅓
IFNAR1 KO
IFNLR1 KO
24 h p.i.
48 h p.i.
72 h p.i.
96 h p.i.
MOI 0.01
MOI 0.1
B
IFN-β before IAV
*
Ratio of the fraction of IAV-positive cells between KO and WT
10
3
1
⅓
IFNLR1 KO
C
IAV (MOI 0.01, 24 h)
IAV, p-STAT1
WT (6.5%)
IFNAR1 KO (8.8%)
IFNLR1 KO (25.5%)
D
IFN-β (100 U/ml, 24 h) before IAV (MOI 1, 24 h)
IAV, p-STAT1
WT (7.0%)
IFNLR1 KO (33.2%)

634

▲ *(continued from the previous page)*

Figure 4. Effect of IFNLR and IFNAR knockout on IAV propagation and activation of immune response

A Fraction of IAV-positive cells in A549 IFNAR1 KO and IFNLR1 KO with respect to the fraction observed for WT. Quantification of three experimental replicates, $p < 0.001$ (***) according to the two-tailed Student *t*-test on log ratios for 24 and 48 h p.i. and MOIs of 0.01 and 0.1 considered jointly.

B Fraction of IAV positive cells in A549 IFNAR1 KO with respect to the fraction observed for WT. Cells were prestimulated with IFN-β at a concentration of 100 U/ml 24 h before infection with IAV at an MOI of 1. Cells were fixed 24 h p.i. Quantification of three experimental replicates, $p < 0.05$ (*), paired two-tailed Student *t*-test on log ratios.

C Representative fields of view (FOV) showing immunostaining for IAV and p-STAT1 in A549 WT, IFNAR1 KO and IFNLR1 KO cells fixed 24 h p.i. with IAV at an MOI of 0.01. Percentages of infected cells in shown FOVs are given in cyan. Scale bar, 100 μm. All immunostaining images are available at Zenodo (see Data availability).

D Representative fields of view (FOV) showing immunostaining for IAV and p-STAT1 in A549 WT and IFNAR1 KO cells prestimulated with IFN-β at a concentration of 100 U/ml 24 h before infection with IAV at an MOI of 1, and fixed 24 h p.i. Percentages of infected cells in shown FOVs are given in cyan. Scale bar, 100 μm. All immunostaining images are available at Zenodo (see Data availability).

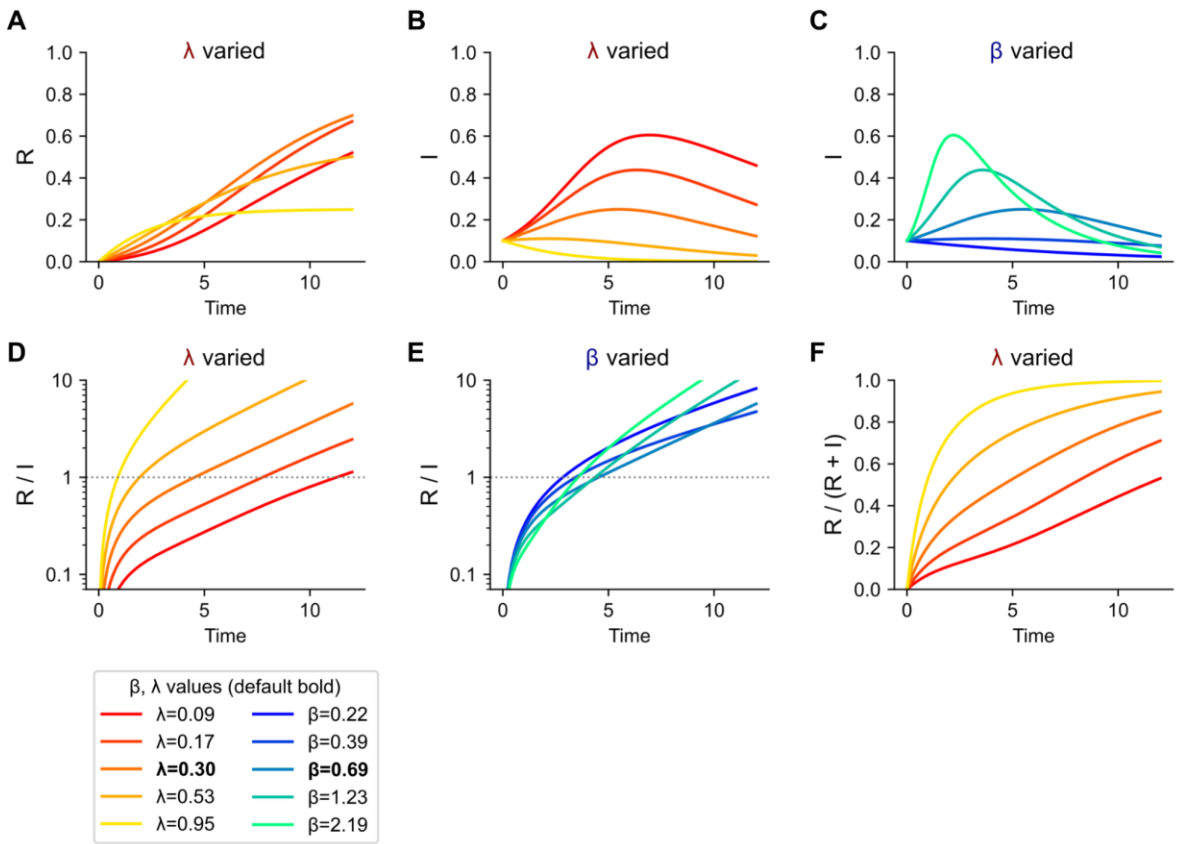

Figure 5. SIR model simulation. Influence of death and infection rates on virus propagation and cell death.

A, **B** Fraction of dead (**A**) or infected (**B**) cells as a function of time and the death rate λ.

C Fraction of infected cells (*I*) as a function of time and the infection rate β.

D, **E** Ratio of dead (*R*) to infected (*I*) fractions as a function of time and the death rate λ (**D**) or the infection rate β (**E**).

F Ratio of dead (*R*) to joint dead and infected (*R* + *I*) fractions as a function of time and the death rate λ.

In all panels, *I*(0) = 0.1, corresponding to MOI = 0.1. Unless specified otherwise, β = 0.69 and λ = 0.3. The default value of β was selected so that the initial doubling time is 1.

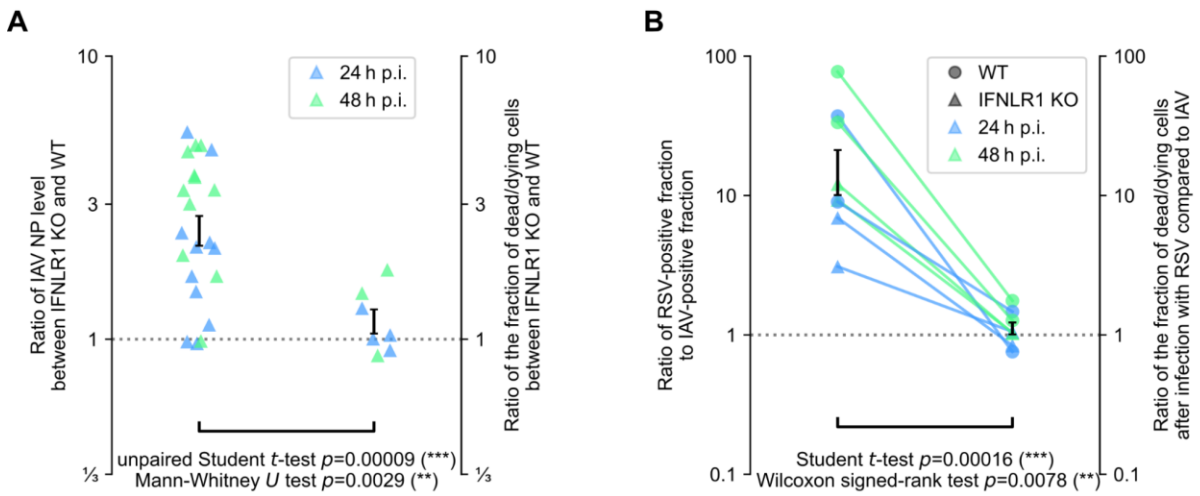

Figure 6. Influence of IFNLR1 deficiency and virus type on infected and dead cell fractions.

A Left: ratio of the IAV NP level between IFNLR1 KO and WT cells – calculated based on Western blots, using cells lysed 24 and 48 h p.i. at an MOI of 0.1. Right: ratio of the fraction of dying/dead cells 24 and 48 h p.i. between IFNLR1 KO and WT – calculated based on cell death assay using annexin V and propidium iodide staining (see Methods). Statistical significance was determined by performing an unpaired two-tailed Student *t*-test and a Mann-Whitney *U* test on log ratios (left *versus* right).

B Left: ratio of RSV-positive to IAV-positive cell fraction at 24 or 48 h p.i. at an MOI of 0.1 – calculated based on immunostaining images (with staining against respectively RSV and IAV). Right: ratio of the fraction of dead/dying cells after infection with RSV to an analogical fraction after infection with IAV. The dead/dying cells were counted based on the propidium iodide signal during live microscopy experiments lasting 24 or 48 h p.i. The same cells were fixed and immunostained to determine the fraction of virus-infected cells used in the left part of the panel. Statistical significance was determined by performing a two-tailed Student *t*-test and a two-tailed Wilcoxon signed-rank test on log ratio-of-ratios (left / right, see Methods).

Supplementary Figure legends

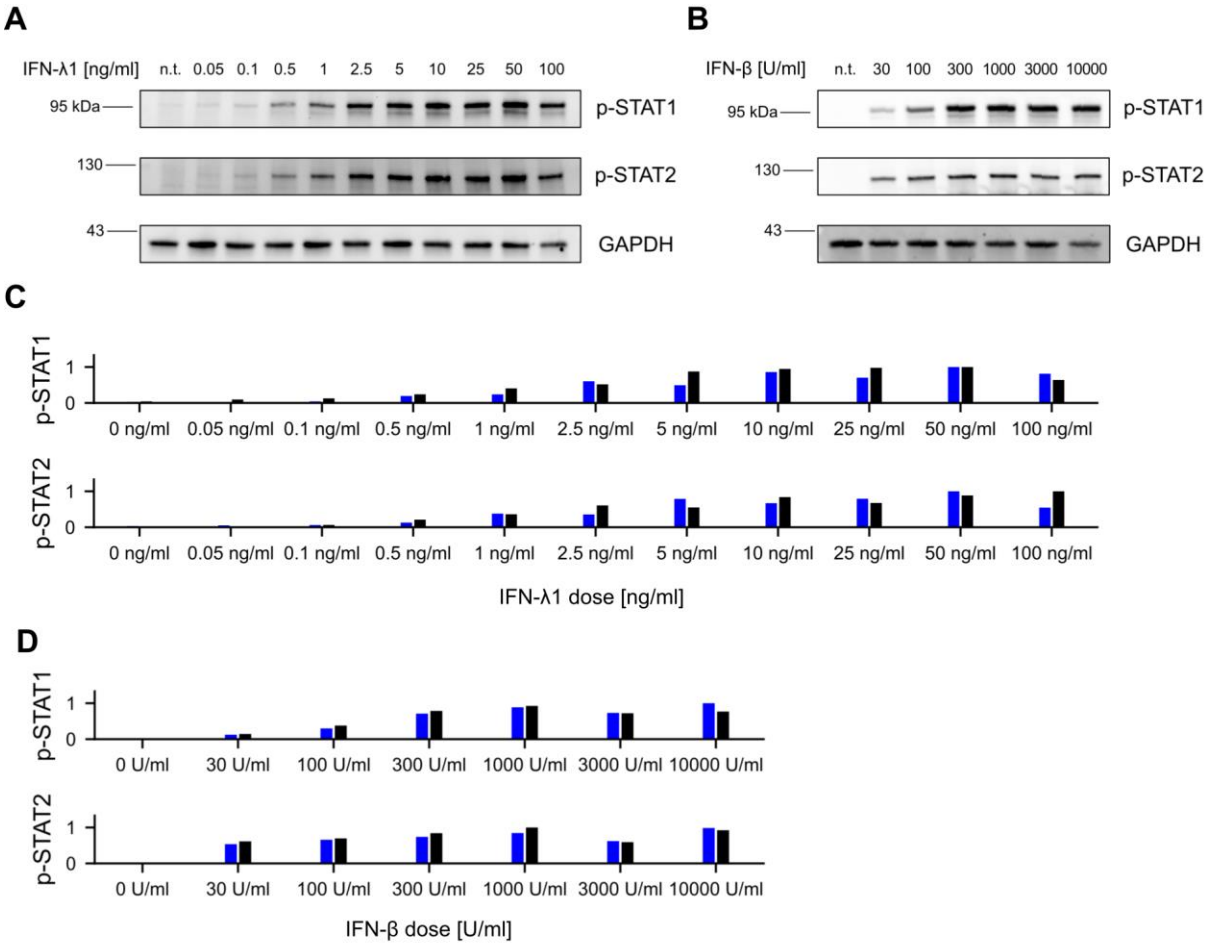

Figure S1. IFN-β and IFN-λ dose–response analysis, determination of saturating concentrations.

A Cells were stimulated with an array of concentrations of IFN-λ1 for 30 min before lysis.

B Cells were stimulated with an array of concentrations of IFN-β for 30 min before lysis.

C Quantification of 2 experimental replicates, blot shown in panel A is marked in blue.

D Quantification of 2 experimental replicates, blot shown in panel B is marked in blue.

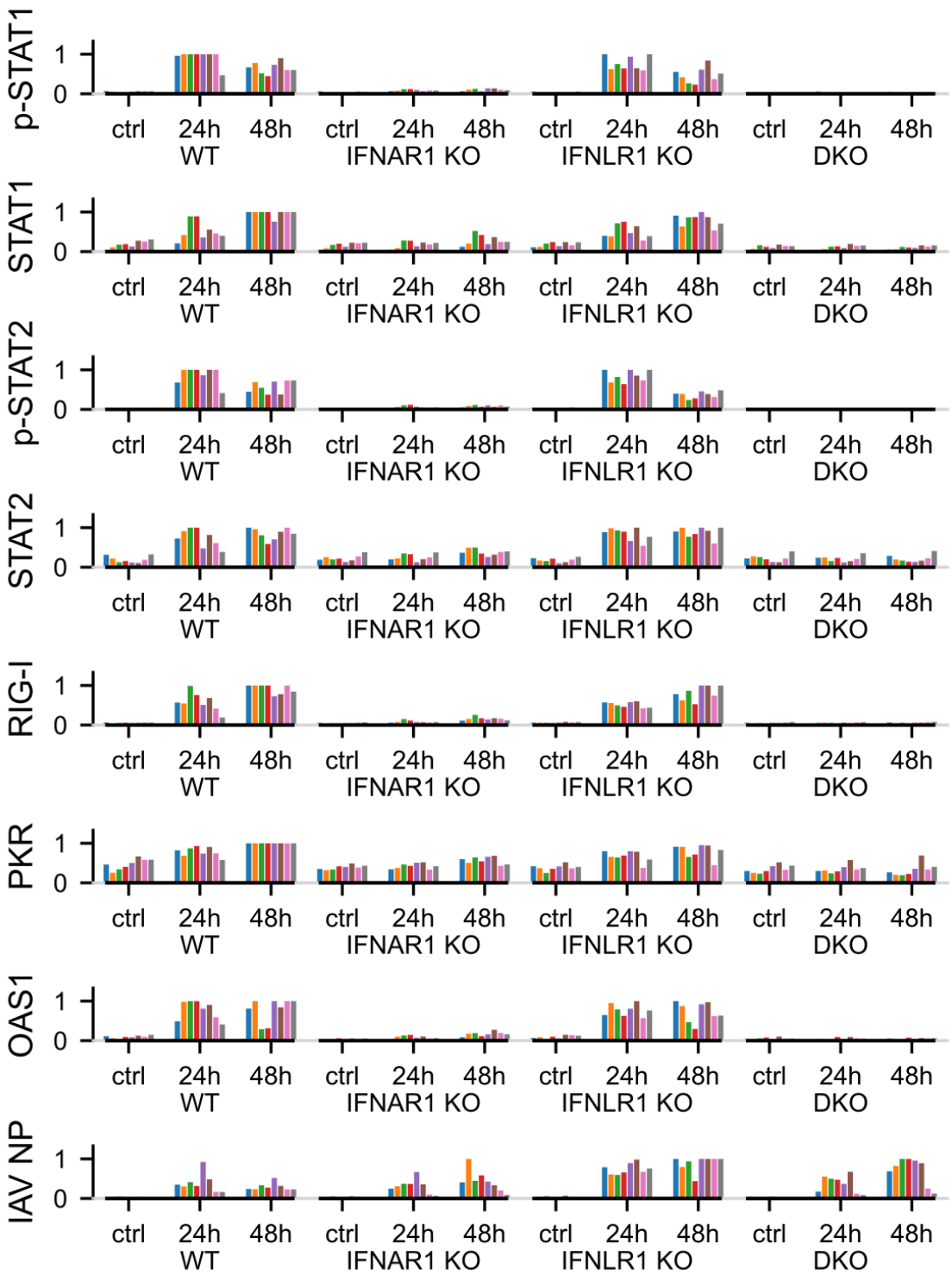

Figure S2. Effect of IFNLR1 and IFNAR1 knockout on IAV proliferation and activation of the innate immune response – full quantification of experiments shown in Fig. 3A.

Colors correspond to independent experimental replicates of experiments shown in Fig. 3A.

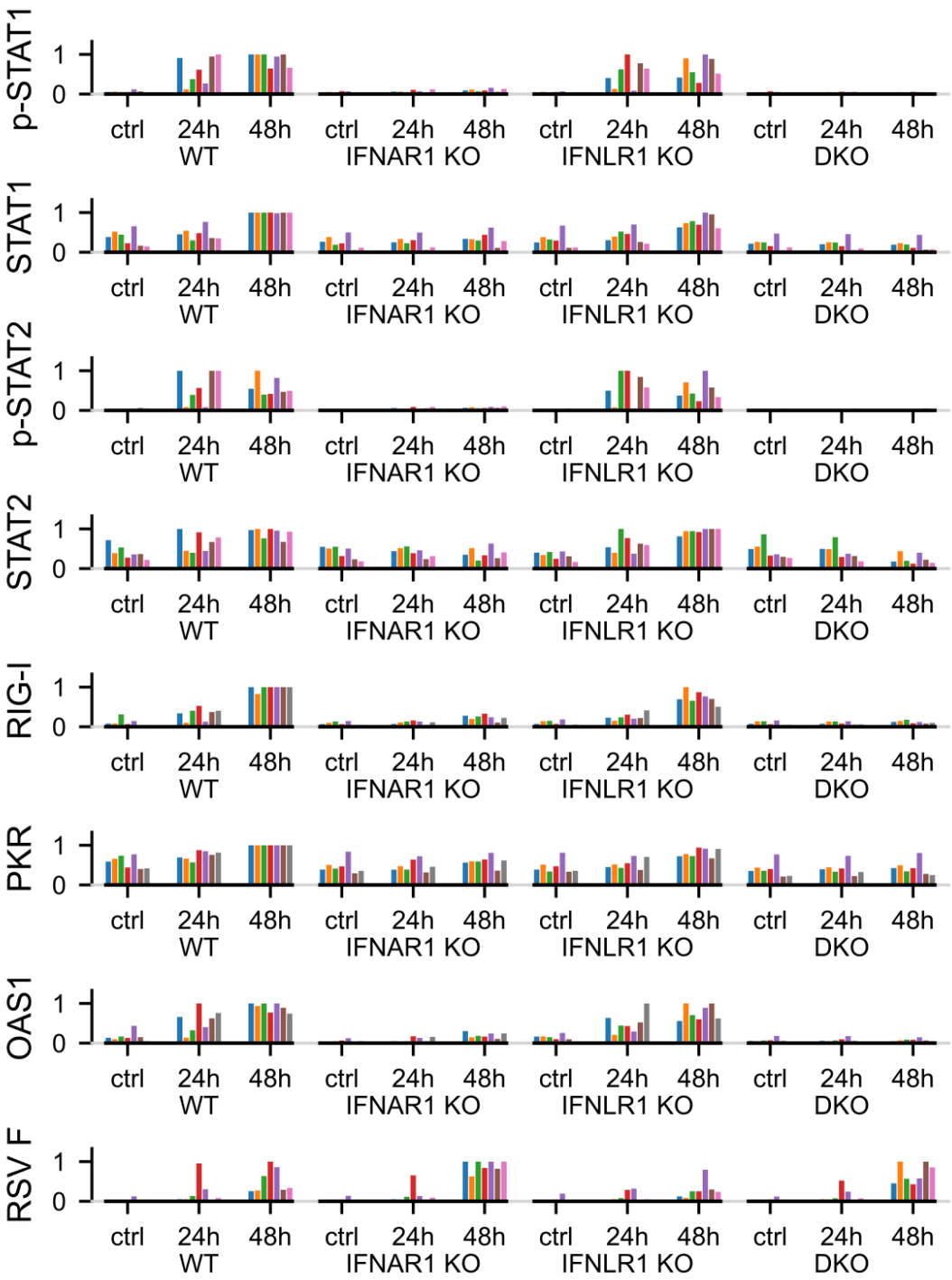

Figure S3. Effect of IFNLR1 and IFNAR1 knockout on RSV proliferation and activation of the innate immune response – full quantification of experiments shown in Fig. 3B.

Colors correspond to independent experimental replicates of experiments shown in Fig. 3B.

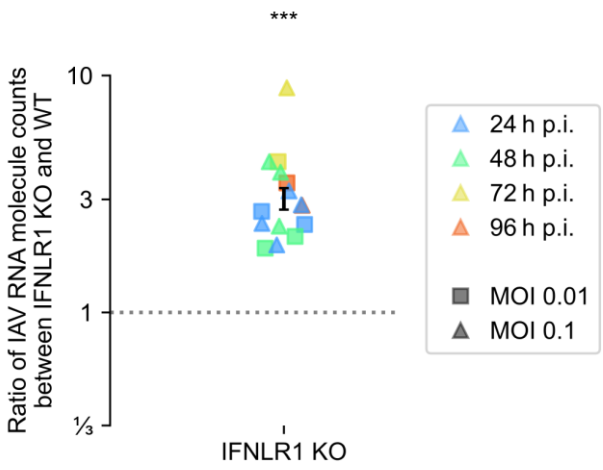

Figure S4. Effect of IFNLR1 deficiency on IAV RNA expression.

Levels of IAV RNA were measured by dPCR for A549 WT and IFNLR1 KO cells at 24, 48, 72 and 96 h p.i. at MOIs of 0.01 and 0.1 (as indicated by the legend). Each square/triangle corresponds to an experimental replicate. Triple asterisk (***) indicates that IAV RNA expression is significantly higher in IFNLR1 KO cells than in WT cells ($p < 0.001$, paired two-tailed Student *t*-test on log ratios).

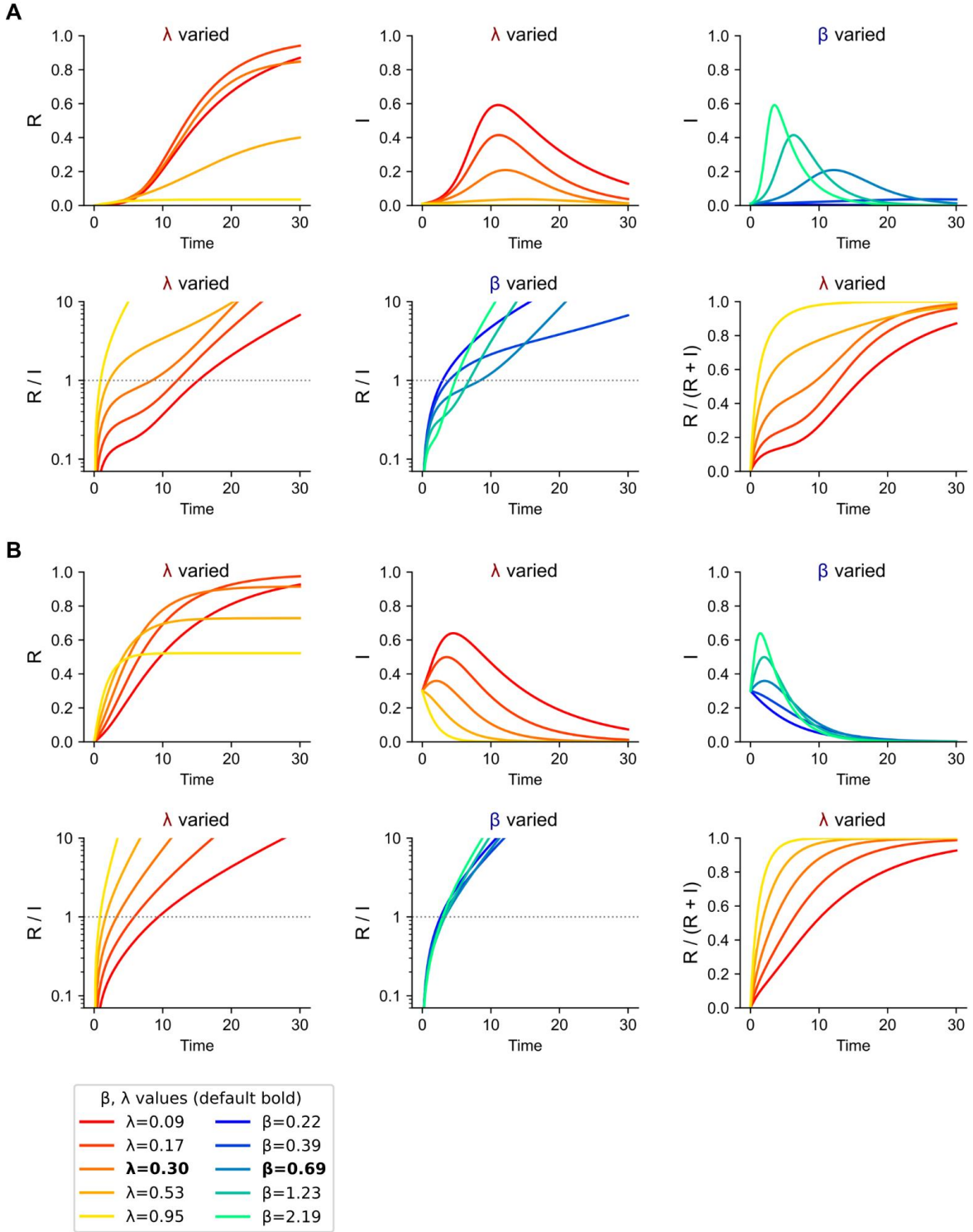

Figure S5. Kinetics of infections in the SIR model. The figure supplements Fig. 5 with data for an MOI of 0.01 (A) and 0.3 (B).

Supplementary Data

Source Data S1 (PDF File). Images of all Western blot replicates.

Source Data S2 (Zipped folder). Data quantifications in CSV format (Western blots, dPCR, RT-PCR, FACS, cell counts from immunostaining) and Python codes to generate figures.